

Vapor-Liquid Phase Coexistence of Alkane–Carbon Dioxide and Perfluoroalkane–Carbon Dioxide Mixtures

S. T. Cui,* H. D. Cochran, and P. T. Cummings

Department of Chemical Engineering, University of Tennessee, Knoxville, Tennessee 37996-2200,
and Chemical Technology Division, Oak Ridge National Laboratory, Oak Ridge, Tennessee 37831-6224

Received: October 23, 1998; In Final Form: March 9, 1999

We carried out a molecular simulation study of the vapor–liquid equilibria of alkane–CO₂ and perfluoroalkane–CO₂ binary mixtures using the Gibbs ensemble Monte Carlo method. We used simple interaction site models and the conventional Lorentz–Berthelot combining rules for the cross interaction between the solute and solvent species with no adjustable parameters to predict the vapor–liquid phase equilibrium of the hexane–CO₂ and perfluorohexane–CO₂ mixtures. The predicted CO₂ mole fraction on the liquid branch is higher than the experimental results by about 10–13%. The gas-phase solubility of hexane and perfluorohexane in CO₂ is generally smaller than the experimental results. The model predicts a higher solubility for the perfluoroalkanes in CO₂ in comparison with alkanes in CO₂, consistent with experiment. The simulation results suggest that the dispersion interaction and the geometric packing may have a predominant role in accounting for the solubility difference between alkane and perfluoroalkane in CO₂.

I. Introduction

Both government and industry are seeking benign substitutes for the many organic solvents used in industry. Solvents are used as media for cleaning, for chemical reactions, and for chemical separation, and most of the solvents used are hazardous to health, safety, and the environment. Supercritical carbon dioxide (SC-CO₂) is often considered as an ideal solvent substitute, but several important classes of substances—water and hydrophilic substances; proteins, nucleic acids, and many other biomolecules; and most man-made high polymers, for example—exhibit very low solubility in SC-CO₂. This has led to an extensive search for effective surfactants that could be used to stabilize microdispersions of water or polymers in SC-CO₂. In analogy to well-known surfactants which stabilize microdispersions in oil–water systems, surfactants for use in SC-CO₂ would be amphiphilic with one part of the surfactant molecule being CO₂-philic. To date, the most successful surfactants for use in SC-CO₂ have contained perfluorinated chains as the CO₂-philic part.^{1,2} Indeed, perfluorinated polymers are among the rare polymers having high solubility in SC-CO₂. Because surfactants in SC-CO₂ form micelles in which the hydrophilic part of the surfactant is in the core, these micelles are generally referred to as reversed micelles (RMs) by analogy to the nomenclature of conventional oil-in-water systems.

The formation of RMs in SC fluids was first reported more than a decade ago,³ and RMs in SC-CO₂ have recently been exploited for heterogeneous polymerizations^{4–15} based on the use of copolymers with poly(1,1-dihydroperfluorooctylacrylate) (PFOA) as surfactant. Perfluoropolyethers have been found to be among the most CO₂-soluble compounds currently available and have been the basis of a number of surfactants.^{15–17} The recently discovered surfactants which support RMs containing water^{5,8,12,18–22} have stimulated considerable research.

The selection of surfactants for water-in-oil RMs in conventional and even SC alkane solvents^{23–25} is reasonably well-understood, but our limited understanding of the ability of surfactants to stabilize the water/SC-CO₂ interface^{15,16,19} has,

so far, yielded systems with only limited water capacity despite a decade-long survey^{26,27} of more than 150 surfactants. Still, spectroscopic studies (shift of the absorbance maximum of methyl orange) indicated the water in the core of a RM exhibited “bulklike” properties, and traces of protein (0.7 equiv/mL of BSA) appear to have been dissolved.²¹

A common feature for all surfactants that have been found so far is that they all contain a fluorinated carbon tail. Although this has served as a guide for investigators in their search for effective CO₂ surfactants, very little is known about the underlying mechanism of interaction between the fluorinated carbon chain and the CO₂ molecules. In this work we seek some molecular-level understanding of why perfluorinated chains are exceptionally CO₂-philic. This is part of a broader search to understand what characteristics lead to successful surfactants for use in SC-CO₂, in hopes of guiding the development of new, improved surfactants. The first step in pursuing this molecular-level understanding is to explore the question of whether some specific interaction is required between perfluorinated compounds and CO₂ to explain their exceptional solubility. We address this question for the perfluoroalkanes, perfluorohexane in particular, for which experimental vapor–liquid phase equilibrium data are available for mixtures with CO₂. Infrared spectroscopic studies²⁸ found no indication of a specific perfluoroalkane–CO₂ interaction. Early *ab initio* molecular modeling calculations²⁹ suggested a specific electrostatic interaction in the perfluoroethane–CO₂ system that was absent in the ethane–CO₂ analogue. However, recent more accurate calculations³⁰ reached the opposite conclusion, i.e., the attraction between the ethane–CO₂ was stronger than that of the perfluoroethane–CO₂ system, and suggested that the dispersion interaction might be dominant. *Ab initio* calculation has not been performed for mixtures of CO₂ with compounds having more than two carbons, and it is not known whether the conclusion can be generalized to longer carbon compounds–CO₂ systems. We also note that miscibility of a binary system involves the

TABLE 1: Potential Models

type of interaction	potential function	parameters
Alkane		
nonbonded interaction	$U_{\text{LJ}}(r_{ij}) = 4\epsilon_{ij} \left\{ \left(\frac{\sigma_{ij}}{r_{ij}} \right)^{12} - \left(\frac{\sigma_{ij}}{r_{ij}} \right)^6 \right\}$	$\sigma_{\text{CH}_3} = \sigma_{\text{CH}_2} = 3.93 \text{ \AA}$ $\epsilon_{\text{CH}_3} = 114 \text{ K}$, $\epsilon_{\text{CH}_2} = 47 \text{ K}$
bond bending	$U_{\text{bb}}(\theta) = 1/2 k_\theta (\theta - \theta_{\text{eq}})^2$	$k_\theta = 62500 \text{ K/rad}^2$ $\theta_{\text{eq}} = 114^\circ$
torsion	$U_{\text{torsion}}(\phi) = a_1(1 + \cos \phi) + a_2(1 - \cos 2\phi) + a_3(1 + \cos 3\phi)$	$a_1 = 355.03 \text{ K}$, $a_2 = -68.19 \text{ K}$ $a_3 = 791.32 \text{ K}$
Perfluoroalkane		
nonbonded interaction	$U_{\text{LJ}}(r_{ij}) = 4\epsilon_{ij} \left\{ \left(\frac{\sigma_{ij}}{r_{ij}} \right)^{12} - \left(\frac{\sigma_{ij}}{r_{ij}} \right)^6 \right\}$	$\sigma_{\text{CF}_3} = \sigma_{\text{CF}_2} = 4.65 \text{ \AA}$ $\epsilon_{\text{CF}_3} = 95 \text{ K}$, $\epsilon_{\text{CF}_2} = 30 \text{ K}$
bond bending	$U_{\text{bb}}(\theta) = 1/2 k_\theta (\theta - \theta_{\text{eq}})^2$	$k_\theta = 62500 \text{ K/rad}^2$ $\theta_{\text{eq}} = 114.6^\circ$
torsion	$U_{\text{torsion}}(\phi) = a_0 + a_1 \cos \phi + a_2 \cos^2 \phi + a_3 \cos^3 \phi + a_4 \cos^4 \phi + a_5 \cos^5 \phi + a_6 \cos^6 \phi + a_7 \cos^7 \phi$	$a_0 = 959.4 \text{ K}$, $a_1 = -282.7 \text{ K}$ $a_2 = 1355.2 \text{ K}$, $a_3 = 6800.0 \text{ K}$ $a_4 = -7875.3 \text{ K}$, $a_5 = -14168.0 \text{ K}$ $a_6 = 9213.7 \text{ K}$, $a_7 = 4123.7 \text{ K}$
Carbon Dioxide (EPM Model) ^a		
Lennard-Jones interaction	$U_{\text{LJ}}(r_{ij}) = 4\epsilon_{ij} \left\{ \left(\frac{\sigma_{ij}}{r_{ij}} \right)^{12} - \left(\frac{\sigma_{ij}}{r_{ij}} \right)^6 \right\}$	$\epsilon_{\text{c-c}} = 28.999 \text{ K}$, $\sigma_{\text{c-c}} = 2.785 \text{ \AA}$ $\epsilon_{\text{o-o}} = 82.997 \text{ K}$, $\sigma_{\text{o-o}} = 3.064 \text{ \AA}$ $\epsilon_{\text{c-o}} = 49.060 \text{ K}$, $\sigma_{\text{c-o}} = 2.921 \text{ \AA}$
charged interaction	$U_{\text{qq}}(r_{ij}) = \frac{q_i q_j}{r_{ij}}$	$q_{\text{c}} = +0.6645e$
bond length		$l_{\text{c-o}} = 1.161 \text{ \AA}$
Carbon Dioxide (EPM2 Model) ^b		
Lennard-Jones interaction	$U_{\text{LJ}}(r_{ij}) = 4\epsilon_{ij} \left\{ \left(\frac{\sigma_{ij}}{r_{ij}} \right)^{12} - \left(\frac{\sigma_{ij}}{r_{ij}} \right)^6 \right\}$	$\epsilon_{\text{c-c}} = 28.129 \text{ K}$, $\sigma_{\text{c-c}} = 2.757 \text{ \AA}$ $\epsilon_{\text{o-o}} = 80.507 \text{ K}$, $\sigma_{\text{o-o}} = 3.033 \text{ \AA}$ $\epsilon_{\text{c-o}} = 47.588 \text{ K}$, $\sigma_{\text{c-o}} = 2.8921 \text{ \AA}$
charged interaction	$U_{\text{qq}}(r_{ij}) = \frac{q_i q_j}{r_{ij}}$	$q_{\text{c}} = +0.6512e$
bond length		$l_{\text{c-o}} = 1.1491 \text{ \AA}$

^a Carbon dioxide is modeled as a rigid linear molecule. The intermolecular interactions are described by the Lennard–Jones interaction and the Coulombic interaction between partial charge sites. ^b EPM2 model was obtained by scaling the parameters of the EPM model to give exact critical properties and is thus an improvement over the EPM model (ref 38).

properties of pure components; thus a complete analysis should also take into account the pure component properties.

We have employed molecular simulation with simple interaction-site models to explore the effects of van der Waals interactions between hexane and CO₂ and between perfluorohexane and CO₂. In the next section, we describe the models and the simulation methods that we used. The subsequent section presents results on pure, single-component systems. Following this are presented results on the binary mixtures of hexane and perfluorohexane with CO₂. We end with some brief concluding remarks.

II. Models and Simulation Details

Simple interaction-site models and the Gibbs ensemble method^{31,32} were used to study the phase coexistence of alkane–CO₂ and perfluoroalkane–CO₂ mixtures. An efficient sampling technique, the configurational bias method,^{33–37} was used for the insertion of chain molecules; the insertion of the CO₂ molecules was accomplished using the ordinary insertion technique. For CO₂, we used the EPM2 model of Harris and Yung,³⁸ which accurately predicts the vapor–liquid-phase equilibria of CO₂. For the majority of the calculations carried out involving alkanes, we used the model developed by Siepmann, Karaborni, and Smit (SKS).^{34,35} For hexane, the SKS model for alkanes accurately predicts the saturated liquid density but underestimates the saturated vapor pressure in comparison to experiment. This may be due to the fact that it was later

realized that there was an error in the calculation of the long range correction in the original work.³⁹ For this reason, we also slightly adjusted the parameters of the SKS model so that the saturated liquid density and vapor pressure can be accurately produced. Calculations were performed using the modified potentials to test how they will affect the phase boundary of the mixture. For perfluoroalkanes, we used a model based on the recent Siepmann model⁴⁰ (referred to as the M-model in the original publication). We slightly adjusted the energy parameter for the CF₃ group of the original Siepmann model to precisely reproduce the vapor pressure and the saturated liquid density. In this way, we can more unambiguously identify the origin of the miscibility behaviors of the two different chain molecules in CO₂ and understand any discrepancy between simulation and experimental results. For convenience to the reader, the models together with their parameters are tabulated in Table 1.

One of the slight complications with using the models for the systems studied in this work is that different truncations were applied in the original models. For alkanes, the interactions were truncated at 14.0 Å, and an average long range correction was applied for distance beyond this cutoff.^{34,35} For CO₂, the original model used a cutoff of 10.0 Å, and an average long range correction was applied beyond this distance.³⁸ In the present study, to be consistent, we have chosen to use a truncation distance of 14.0 Å for all models, so that the cross interaction can be truncated at the same distance. Long range

TABLE 2: Vapor–Liquid-Phase Equilibrium Results for EPM and EPM2 Models for CO₂

T (K)	density (kg/m ³)									
	EPM model				EPM2 model					
	Harris and Yung ^a		this work		Errington et al. ^b		this work		experiment ^c	
	liquid	vapor	liquid	vapor	liquid	vapor	liquid	vapor	liquid	vapor
238	1164 (4)	23.7 (2.0)	1072 (4)	24.7 (1.6)	1084 (7)	29.4 (2.4)	1071 (5)	29.3 (1.4)	1094.9	31.2
248					1045 (11)	44.3 (3.0)	1036 (6)	46.3 (5.3)	1052.6	43.7
258	996.9 (3)	49.4 (1.3)	996.0 (4.5)	46.3 (2.4)					1006.1	60.2
268					949.6 (7.9)	83.7 (5.3)	944.0 (7.0)	89.7 (2.0)	956.5	82.4
278	909.6 (3)	89.6 (7.4)	901.7 (8.0)	88.6 (5.8)					898.5	114.7

^a Reference 38. ^b Reference 42. ^c Reference 44.

corrections were applied to all interactions. The original Harris and Yung model³⁸ also has site charges to take into account the quadrupole moment of the CO₂ molecule. They used a 10.0 Å cutoff in combination with a site–site reaction field to treat the long range electrostatic interaction. The authors noted in their original paper that the cutoff distance should be considered a part of their model. Since a long range correction has been applied to the Lennard–Jones interaction in their work, this part of the potential can be considered essentially independent of the cutoff distance. For the mixtures studied in this work, only CO₂ has charges so there is no interspecies electrostatic interaction. Thus, we have kept the electrostatic part of the model unchanged (i.e., a cutoff distance of 10.0 Å for the CO₂ charge–charge interaction with site–site reaction field correction), so that the change to the phase behavior of the original model due to the alteration of the Lennard–Jones cutoff distance is negligible, as will be seen below. The performance of the models described above in predicting pure system vapor–liquid phase behavior is discussed in the next section.

For the cross interactions between alkanes and CO₂ and between perfluoroalkanes and CO₂, the Lorentz–Berthelot combining rules are used, i.e., the energy parameter between interaction sites of difference species is determined by the geometric mean $\epsilon_{ij} = \sqrt{\epsilon_i \epsilon_j}$, and the size parameter is determined by the arithmetic mean $\sigma_{ij} = 1/2(\sigma_i + \sigma_j)$.

Initial configurations were obtained by putting the center of mass of molecules on a cubic lattice. For mixtures at high pressures, CO₂ molecules were placed on lattice points first. Chain molecules were then placed in the simulation volume. When there was overlap between a CO₂ molecule and a chain molecule, the CO₂ molecule was deleted from the volume. At low pressures, an alternative method for setting up the initial configuration was used. Two separate volumes of alkane-rich (perfluoroalkane-rich) or CO₂-rich systems were created, and the molecules were allowed to mix after initial equilibration. The alkane-rich (perfluoroalkane-rich) system was produced by placing the alkane molecules in the volume first and then randomly inserting the CO₂ molecules to the simulation volume. The CO₂-rich system was produced as in the high-pressure case. The total number of molecules used varies between 202 for the lowest pressure and 1080 at high pressure in the simulations. The initial composition was chosen to be between the experimental compositions of the vapor and liquid branches.

III. Properties of Pure Systems

1. Carbon Dioxide. The performance of the CO₂ model (EPM and EPM2 models)³⁸ was calculated at a few representative temperatures, as listed in Table 2, together with experimental data⁴⁴ and published simulation results from other groups.⁴² The table shows that for pure CO₂, the EPM2 model yields very good agreement with experiment. We tested the

effect of altering the cutoff distance on the vapor–liquid-phase behavior for the EPM model. At 258 K, using a cutoff distance of 14.0 Å, we obtained the saturated liquid and vapor densities of 1001 and 47.5 kg/m³, compared to the corresponding saturated liquid and vapor densities of 996 and 46.3 kg/m³ using a cutoff distance of 10.0 Å.

2. Perfluoroalkanes. We have chosen the model for perfluoroalkanes to best reproduce the vapor pressure and saturated liquid density of perfluorohexane. We used a model based on the model of Siepmann (referred to as the M-model in ref 40), with a slight reduction of the CF₃ energy parameter (from 100 to 95 K) to obtain good prediction for the saturated liquid density and vapor pressure for phase equilibrium. The energy parameter for the CF₂ group has been shown to best reproduce the scaling behavior for critical temperature and density as the chain length varies.⁴⁰ We point out that the present model includes long range correction while the original Siepmann model simply used a truncation at 14.0 Å without long range correction. The intramolecular bending and torsional potentials are those of the T-model in the paper by Cui et al.⁴⁰ The results for perfluorohexane are shown in Figure 1. In Figure 1a, vapor pressure of the model is plotted versus temperature together with experimental data.⁴¹ In Figure 1b, the saturated liquid density of the model prediction is plotted together with experimental data. As can be seen, the simulation using $\epsilon_{CF_3} = 95$ K yields saturated liquid densities which agree with experiment to better than 2%, while the vapor pressures almost completely agree with experiment. However, the temperature dependence of the saturated liquid density from simulation shows a somewhat different slope from that of the experiment, reflecting the fact that state condition-dependent potential parameters may be needed to more satisfactorily predict the vapor–liquid phase equilibria.

3. Alkanes. Figure 2 presents the saturated liquid density and vapor pressure for hexane calculated using the SKS model^{34,35} and some slight variations of the model, along with experimental data.⁴³ The SKS model for alkanes gives a reasonable saturated liquid density but significantly lower vapor density and hence lower vapor pressure at temperatures when the ideal gas part dominates. Our calculation at 372 K, for example, yields a saturated vapor density $\rho_v = 0.0047$ g/cm³, a saturated liquid density $\rho_l = 0.585$ g/cm³, and a saturated vapor pressure $P_v = 0.158$ MPa, compared to the experimental values of $\rho_v = 0.0073$ g/cm³, $\rho_l = 0.581$ g/cm³, and $P_v = 0.239$ MPa. Thus, for the purpose of analyzing the mixture results, we also carried out simulations using slightly adjusted parameters for the site–site Lennard–Jones potential. In one set of calculations, we slightly decreased the CH₃ group energy parameter only. The model produces a vapor pressure very close to experiment and a slightly lower saturated liquid density. In another calculation, the size parameter is also slightly reduced to produce both a vapor pressure and a saturated liquid density which are very close to

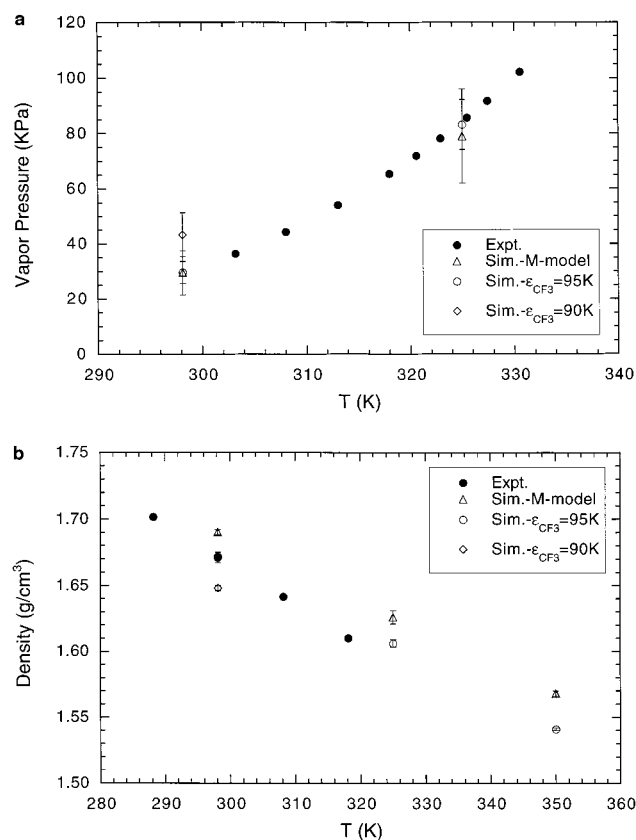


Figure 1. (a) Vapor pressure for perfluorohexane. Solid circles are experimental results.⁴¹ Triangles are the results of simulation using the Lennard–Jones parameter sets of the M-model.⁴⁰ Open circles are results obtained by reducing the CF₃ group Lennard–Jones energy parameter of the M-model to $\epsilon/k_B = 95$ K. Diamonds are results obtained by further reducing the CF₃ group energy parameter to $\epsilon/k_B = 90$ K. (b) Saturated liquid density of perfluorohexane. Symbols have the same meaning as in panel a.

experiment, as can be seen from the figures. The effect of these variations on the mixture properties will be discussed in the next few sections.

IV. Hexane–CO₂ and Perfluorohexane–CO₂ Mixtures

In Figure 3a, we present the solubility of hexane with CO₂ at 40 °C from simulation together with experimental data.^{28,45} On the gas-phase branch at moderate pressure, the solubility of hexane in CO₂ from simulation is very low, in agreement with the corresponding experimental results. On the liquid branch of the phase diagram, the mole fraction of CO₂ from simulation is generally higher than the corresponding experimental data. The largest deviations are from the middle range of the pressure, where the mole fraction of CO₂ from simulation is about 13% larger than experiment.

Data points using the slightly modified model for the hexane are also plotted in Figure 3a. They show what might be expected from a model more accurately describing the pure hexane phase behavior than the SKS model. The result is that the effect is relatively small for both the liquid-phase and the gas-phase branches. When reducing the energy parameter for the CH₃ groups to 105 K while keeping all other parameters unchanged, the mole fraction of CO₂ in the liquid phase is increased by about 1–2%. When also slightly decreasing the size parameter from $\sigma = 3.93$ to 3.91 Å to reproduce more accurately the saturated liquid density for hexane (see Figure 2), the data point at 4.0 MPa pressure essentially coincides with the result using the SKS model.

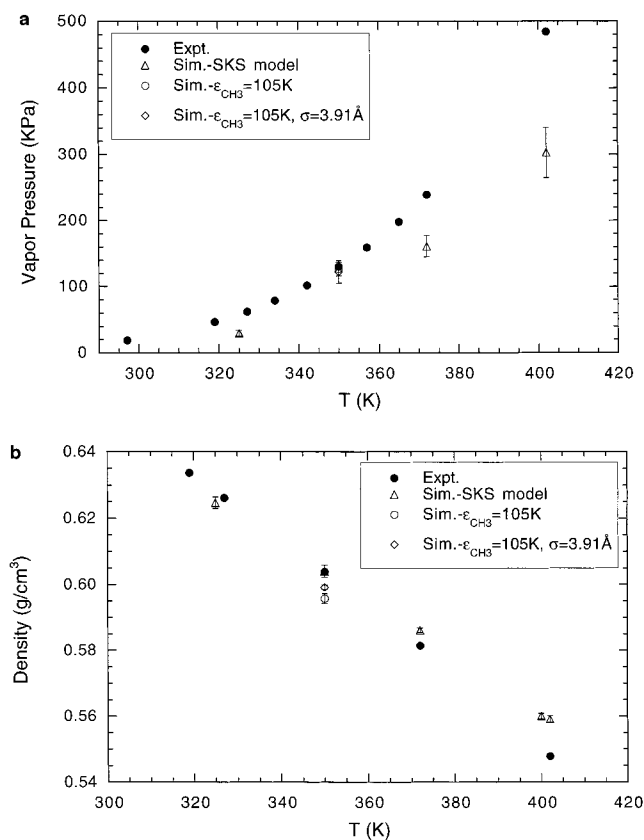


Figure 2. (a) Vapor pressure for hexane. Solid circles are experimental results.⁴² Triangles are the results of simulation using the SKS model.^{34,35} The open circle is the result obtained by reducing the Lennard–Jones energy parameter for the CH₃ group to $\epsilon/k_B = 105$ K. The diamond is the result obtained by reducing the Lennard–Jones energy parameter of the CH₃ group to $\epsilon/k_B = 105$ K and the size parameter to $\sigma = 3.91$ Å (note that in this model CH₃ and CH₂ groups have the same size parameter). (b) Saturated liquid density for hexane. Symbols have the same meaning as in panel a.

Figure 3b shows similar phase equilibrium results from simulation and experiment⁴⁵ for C₆H₁₄ in CO₂ at 80 °C. On the gas-phase branch in the moderate pressure range, the mole fraction of hexane in CO₂ from simulation is slightly smaller than experiment, 3–4% in comparison to the experimental data of about 5–6%. On the liquid branch in the moderate pressure range, the mole fraction of CO₂ in hexane is about 10% higher. At high pressure, the gas-phase CO₂ mole fraction from simulation has a tendency to increase slightly, while this is absent from the experimental data. This may reflect the inadequacy of the state condition independence of the parameters used in the models. Another possible reason for the observed behavior in simulation may be the finite size effect in the simulated systems which becomes more severe as the critical point is approached where the correlation length becomes very long. On the experimental side, impurities might also affect the experimentally measured phase equilibria at high pressures near the critical point, especially if lower molecular weight hydrocarbons were present. Other published works⁴⁶ indicate that the above observed tendency for the gas-phase branch could happen for mixtures with high asymmetry in molecular size. In comparing parts a and b of Figure 3, both simulation and experimental results show that increasing the temperature from 40 to 80 °C decreases the miscibility of hexane and CO₂, as can be seen by the larger miscibility gap as the temperature increases.

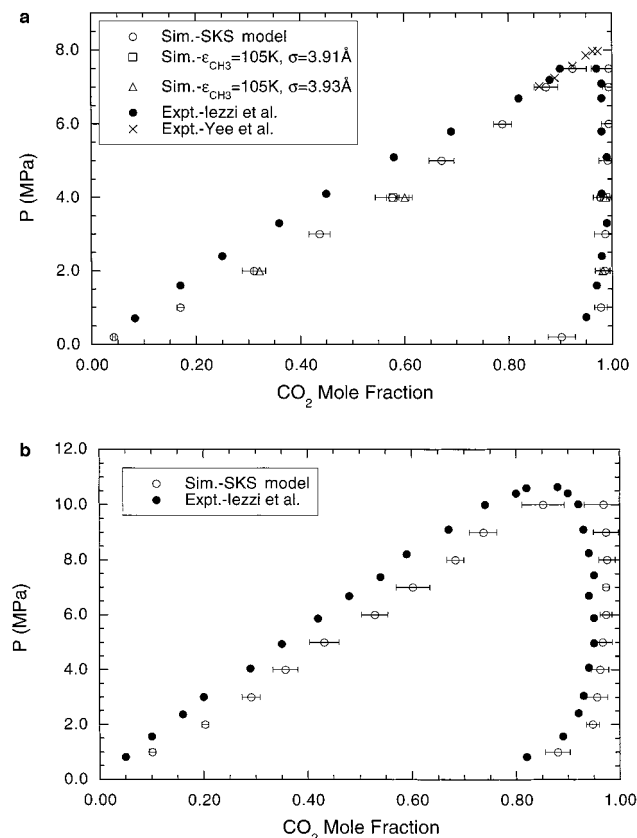


Figure 3. (a) Vapor-liquid phase diagram for C₆H₁₄-CO₂ mixture at 40 °C. Solid circles are the experimental data of Iezzi et al.⁴⁵ Crosses are the experimental data of Yee et al.²⁸ Open circles are simulation results obtained using the SKS model^{34,35} for hexane. Triangles are results obtained by slightly reducing the CH₃ group energy parameter to 105 K. Squares are results obtained by varying the CH₃ group energy parameter to 105 K and the hexane Lennard-Jones size parameter (for both CH₃ and CH₂) to 3.91 Å. (b) Vapor-liquid phase diagram for C₆H₁₄-CO₂ mixture at 80 °C. Solid circles are experimental data of Iezzi et al.⁴⁵ Open circles are results of simulation using the SKS model.

Figure 4a shows the phase diagram for perfluorohexane at 41.5 °C from simulation, together with experimental data⁴⁵ at the same temperature and some experimental data at 40 °C.²⁸ On the gas-phase branch of the coexistence curve, the solubility of perfluorohexane in CO₂ from simulation is close to experiment but slightly lower. On the liquid branch, as for the case of hexane-CO₂, the simulation again overestimates the solubility of CO₂ in perfluorohexane. The difference is about 13% between the simulation and the experiment in mole fraction of CO₂ in perfluorohexane.

Figure 4b shows the phase diagram of the same perfluorohexane-CO₂ system at a higher temperature, $T = 81.1$ °C, together with the experimental data.⁴⁵ The agreement between the simulation and experiment is similar to the case of hexane-CO₂ at $T = 80$ °C. The gas-phase branch has slightly higher CO₂ concentration from simulation than experiment. The liquid branch of the phase coexistence from the simulation has a higher CO₂ mole fraction than experiment by about 10%.

For comparison of miscibility of hexane and perfluorohexane with CO₂, we replot in Figure 5 the simulation results from Figures 3a and 4a. Consistent with experiment, the phase diagrams for the two mixtures demonstrate that the perfluorohexane is more miscible with CO₂ than hexane, as seen by the smaller gap between the two phases for the perfluorohexane-CO₂ mixture. The results at higher temperature are not plotted

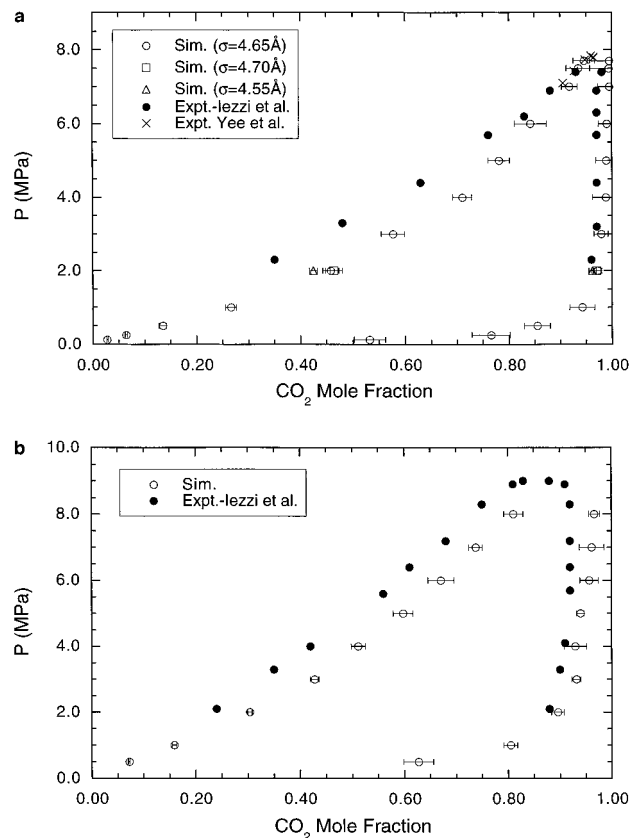


Figure 4. (a) Vapor-liquid phase diagram for C₆F₁₄-CO₂ mixture at 41.5 °C. Solid circles are the experimental data of Iezzi et al.⁴⁵ Crosses are the experimental data of Yee et al.²⁸ Open circles are simulation results obtained using a slight modification of the M-model, as presented in Table 1. Squares are results obtained by slightly increasing the Lennard-Jones size parameter to 4.70 Å. Triangles are results obtained by slightly decreasing the size parameter to 4.55 Å. (b) Vapor-liquid phase diagram for C₆F₁₄-CO₂ mixture at 80.1 °C. Solid circles are the experimental data.⁴⁵ Open circles are the results of simulation using the model presented in Table 1.

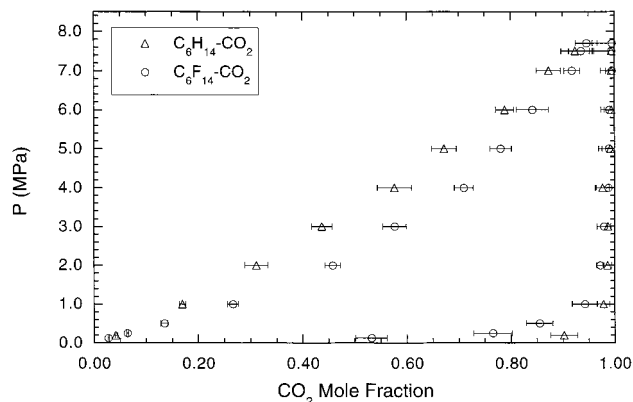


Figure 5. Comparison of miscibility of C₆H₁₄-CO₂ mixture and C₆F₁₄-CO₂ mixtures obtained by simulation using the models presented in Table 1: triangles, C₆H₁₄-CO₂ mixture; circles, C₆F₁₄-CO₂ mixture.

here but show similar behavior, as can be seen by comparing Figures 3b and 4b.

V. Concluding Remarks

In summary, we have considered simple models for the alkanes and perfluoroalkanes in CO₂ and investigated their miscibility. This study may be considered an attempt to elucidate the degree to which the simple dispersion and geometric

considerations can explain the miscibility between alkanes (perfluoroalkanes) and CO₂ thus providing a basis for further refinement and modification of the models. The phase equilibria calculated from simulation are obviously not in quantitative agreement with experiment, especially on the liquid branch. One easy solution to this might be to introduce some adjustable parameters in the combining rules. We have chosen not to introduce the adjustable binary interaction parameters in this study with the objective to seek a more fundamentally based resolution. In view of the simplicity of the models used, it is encouraging that they yield miscibility results which are consistent with the trend of experiment, i.e., the solubility enhancement of the perfluoroalkanes in CO₂ compared to alkanes. The above models therefore provide a starting point for future study of alkane–CO₂ and perfluoroalkane–CO₂ mixtures.

A complete theory of the mixing of perfluoroalkanes with CO₂ is still lacking at the moment, and a satisfactory interpretation for this enhanced solubility has not been established. Some attempts have been made to interpret the mixing behavior of the perfluoroalkanes in CO₂ in terms of the regular solution theory by comparing the solubility parameters, δ , of the perfluoroalkanes and CO₂. For perfluorohexane, $\delta = 5.9$ (cal/cm³)^{1/2}; for CO₂, $\delta = 6.0$ (cal/cm³)^{1/2}; and for hexane, $\delta = 7.3$ (cal/cm³)^{1/2}. Although we did not make any attempt to calculate the solubility parameters for the systems studied here, the fact that the simple interaction-site models correctly predict the increase of the miscibility for perfluoroalkane–CO₂ compared with the alkane–CO₂ mixture indicates that geometric packing and dispersion interactions have a major role on the miscibility in the two mixtures.

It is difficult to judge from the present model whether an electrostatic interaction should be introduced to improve the model for perfluoroalkanes, although the results in this study suggest that the electrostatic interaction between perfluoroalkane and CO₂ may not play a dominant role. We also note that since CO₂ molecules have an electric quadrupole moment, the introduction of site charge or multipole moment will likely enhance the cross interaction between the perfluoroalkanes and CO₂. This will result in an even higher CO₂ solubility in liquid perfluoroalkane unless significant change is made to the parameters of the Lennard–Jones potential. We already mentioned the conflicting results from ab initio quantum calculations on the existence of electrostatic interaction between perfluoroalkanes and CO₂. On the experimental side, the results of Yee et al.²⁸ suggested no existence of a specific interaction between hexane (or perfluorohexane) and CO₂. However, a recent F-19 NMR experiment⁴⁷ suggested the existence of a specific interaction between perfluoroalkane and CO₂. All these suggest that the difference between the alkanes and perfluoroalkanes may be subtle, and further detailed studies, both theoretical and experimental, are needed.

It appears that there is no straightforward way to modify the models for the pure systems to fit to the experimental mixture data while at the same time keeping the simplicity of the Lennard–Jones model and simple combining rules. We have tried a slightly different value for the σ -parameter for hexane and perfluorohexane. By slightly varying the size parameter of the Lennard–Jones potential with $\sigma = 4.55$ and 4.70 Å for perfluorohexane, we obtained the mole fraction of CO₂ on the liquid branch at 41.5 °C and $P = 2.0$ MPa to be 42.5% and 46.4%. The effect on the vapor branch is very slight. These results show that significant reduction to the size parameter of the Lennard–Jones potential of the perfluoroalkane model has

to be made to achieve a satisfactory agreement with experiment for liquid branch miscibility. This will result in a substantially higher saturated liquid density for the pure perfluorohexane. It is also clear from these results that increase of the pure liquid density decreases the solubility of CO₂ in the liquid, as can be understood intuitively.

We comment that the current model for perfluoroalkanes is fairly crude, with no explicit representation for the fluorine atoms. A fluorine atom is significantly larger than a hydrogen atom, so, while a united atom model is adequate for the alkanes, an explicit representation of fluorine atoms in the perfluoroalkane model may be required to more accurately describe the system.

Acknowledgment. We are pleased to acknowledge support for this work by the Chemical and Thermal Systems Division of the National Science Foundation under Grant No. CTS-9613555 at the University of Tennessee and by the Chemical Sciences Division of the Department of Energy at Oak Ridge National Laboratory. Oak Ridge National Laboratory is managed by Lockheed Martin Energy Research Corp. for the Department of Energy under Contract No. DE-AC05-96OR22464.

References and Notes

- (1) Fox, K. C. *Science* **1994**, 265, 321.
- (2) McClain, J. B.; Betts, D. E.; Canelas, D. A.; Samulski, E. T.; DeSimone, J. M.; Londono, J. D.; Cochran, H. D.; Wignall, G. D.; Chillura-Martino, D.; Triolo, R. *Science* **1996**, 274, 2049.
- (3) Gale, R. W.; Fulton, J. L.; Smith, R. D. *J. Phys. Chem.* **1987**, 91, 920.
- (4) DeSimone, J. M.; Guan, Z.; Elsbernd, C. S. *Science* **1992**, 257, 945.
- (5) DeSimone, J. M.; Maury, E. E.; Combes, J. R.; Menciloglu, Y. Z. *PMSE Preprints* **1993**, 68.
- (6) DeSimone, J. M.; Maury, E. E.; Menciloglu, Y. Z.; McClain, J. B.; Romack, T. J.; Combes, J. R. *Science* **1994**, 265, 356.
- (7) Adamsky, F. A.; Beckman, E. J. *Macromolecules* **1994**, 27, 312.
- (8) Guan, Z.; DeSimone, J. M. *Macromolecules* **1994**, 27, 5527.
- (9) Romack, T. J.; DeSimone, J. M.; Treat, T. A. *Macromolecules* **1995**, 28, 8429.
- (10) Romack, T. J.; Kipp, B. E.; DeSimone, J. M. *Macromolecules* **1995**, 28, 8432.
- (11) Clark, M. R.; DeSimone, J. M. *Macromolecules* **1995**, 28, 3002.
- (12) Fulton, J. L.; Pfund, D. M.; McClain, J. B.; Romack, T. J.; Maury, E. E.; Combes, J. R.; Samulski, E. T.; DeSimone, J. M.; Capel, M. *Langmuir* **1995**, 11, 4241.
- (13) Kapellen, K. K.; Mistele, C. D.; DeSimone, J. M. *Macromolecules* **1996**, 29, 495.
- (14) Mistelle, C. D.; Thorp, H. H.; DeSimone, J. M. *JMS—Pure Appl. Chem. A* **1996**, 33, 953.
- (15) Hoeffling, T. A.; Beitle, R. R.; Enick, R. M.; Beckman, E. J. *Fluid Phase Equilib.* **1993**, 83, 203.
- (16) Hoeffling, T. A.; Newman, D. A.; Enick, R. M.; Beckman, E. J. *J. Supercrit. Fluids* **1993**, 6, 205.
- (17) Singley, E. J.; Liu, W.; Beckman, E. J. *Fluid Phase Equilib.* **1997**, 128, 199.
- (18) Maury, E. E.; Batten, H. J.; Killia, S. K.; Menciloglu, Y. Z.; Combes, J. R.; DeSimone, J. M. *Polymer Preprints* **1993**, 34, 664.
- (19) Harrison, K.; Goveas, J.; Johnston, K. P.; O'Rear, E. A. *Langmuir* **1994**, 10, 3536.
- (20) Beckman, E. J. *Science* **1996**, 271, 613.
- (21) Johnston, K. P.; Harrison, K. L.; Clarke, M. J.; Howdle, S. M.; Heitze, M. P.; Bright, F. V.; Carlier, C.; Randolph, T. W. *Science* **1996**, 271, 624.
- (22) Estoe, J.; Bayazit, Z.; Martel, S.; Steytler, D. C.; Heenan, R. K. *Langmuir* **1996**, 12, 1423.
- (23) Kaler, E. W.; Billman, J. F.; Fulton, J. L.; Smith, R. D. *J. Phys. Chem.* **1991**, 95, 458.
- (24) Peck, D. G.; Johnston, K. P. *J. Phys. Chem.* **1991**, 95, 9549.
- (25) McFann, G. J.; Johnston, K. P. *J. Phys. Chem.* **1991**, 95, 4889.
- (26) Iezzi, A.; Enick, R. M.; Brady, J. *ACS Symp. Ser.* **1989**, 406, 122.
- (27) Consani, K. A.; Smith, R. D. *J. Supercrit. Fluids* **1990**, 3, 51.
- (28) Yee, G. G.; Fulton, J. L.; Smith, R. D. *J. Phys. Chem.* **1992**, 96, 6172.
- (29) Cece, A.; Jureller, S. H.; Kerschner, J. L.; Moschner, K. F. *J. Chem. Phys.* **1996**, 100, 7435.

- (30) Diep, P.; Jordan, K. D.; Johnson, J. K.; Beckman, E. J. *J. Phys. Chem. A* **1998**, *102*, 2231.
- (31) Panagiotopoulos, A. Z. *Mol. Phys.* **1987**, *61*, 813.
- (32) Panagiotopoulos, A. Z.; Quirke, N.; Stapleton, M.; Tildesley, D. J. *Mol. Phys.* **1988**, *63*, 527.
- (33) Siepmann, J. I.; Frenkel, D. *Mol. Phys.* **1992**, *75*, 59.
- (34) Siepmann, J. I.; Karaborni, S.; Smit, B. *Nature* **1993**, *365*, 330.
- (35) Smit, B.; Karaborni, S.; Siepmann, J. I. *J. Chem. Phys.* **1995**, *102*, 2126.
- (36) de Pablo, J. J.; Laso, M.; Suter, U. W. *J. Chem. Phys.* **1992**, *96*, 2395.
- (37) Laso, M.; de Pablo, J. J.; Suter, U. W. *J. Chem. Phys.* **1992**, *97*, 2817.
- (38) Harris, J. G.; Yung, K. H. *J. Phys. Chem.* **1995**, *99*, 12021.
- (39) B. Smit, personal communication, 1996. See also: Note Added in Proof, in Siepmann, J. I.; Martin, M. G. *Mol. Phys.* **1997**, *90*, 687.
- (40) Cui, S. T.; Siepmann, J. I.; Cochran, H. D.; Cummings, P. T. *Fluid Phase Equilib.* **1998**, *146*, 51.
- (41) Dunlap, R. D.; Purphy, C. J., Jr.; Bedford, R. G. *J. Am. Chem. Soc.* **1958**, *80*, 84.
- (42) Errington, J. R.; Panagiotopoulos, A. Z. Results posted at the website http://thera.umd.edu/jerring/gibbs/results/co2_emp2/co2_emp2.html.
- (43) Smith, B. D.; Srivastava, R. *Thermodynamic Data for Pure Compounds*; Elsevier Science Publishers B.V.: Amsterdam, 1986.
- (44) Newitt, D. M.; Pai, M. U.; Kuloor, N. R.; Huggill, J. A. W. In *Thermodynamic Functions of Gases*, Din, F., Ed.; Butterworth: London, 1956; Vol. 123.
- (45) Iezzi, A.; Bendale, P.; Enick, R. M. *Fluid Phase Equilib.* **1989**, *52*, 307.
- (46) Georgoulaki, A. M.; Ntouros, I. V.; Dimitrios, P. T.; Panagiotopoulos, A. Z. *Fluid Phase Equilib.* **1994**, *100*, 153.
- (47) Dardin, A.; DeSimone, M. J.; Samulski, E. T. *J. Phys. Chem. B* **1998**, *102*, 1775.